Research on the state of charge estimation method of lithium-ion batteries based on novel limited memory multi-innovation least squares method and SDE-2-RC equivalent model.

CAO, J., WANG, S., XIE, Y. and FERNANDEZ, C.

2023

Research on the state of charge estimation method of lithium-ion batteries based on novel limited memory multi-innovation least squares method and SDE-2-RC equivalent model

Jie Cao[a], Shunli Wang[ab*], Yanxin Xie[a], Carlos Fernandez[c]

[a]*School of Information Engineering, Southwest University of Science and Technology, Mianyang 621010, China;*

[b]*College of Electrical Engineering, Sichuan University, Chengdu 610065, China;*

[c]*School of Pharmacy and Life Sciences, Robert Gordon University, Aberdeen, UK*

Abstract: Because of the common data redundancy phenomenon in the current least-squares parameter identification algorithm and the complex offline parameter identification process, this research innovatively proposes a Limited Memory Multi-Innovation Least Squares (LM-MILS) ternary lithium-ion battery (LIB) parameter identification algorithm that uses a limited set of data to estimate model parameters and attenuates the effects of old data. To improve the parameter fidelity of the equivalent circuit model (ECM) of the LIB, considering that the open-circuit voltage of the lithium-ion battery will gradually decrease with the self-discharge when it is not in use, based on a large number of experiments, a model considering the self-discharge of the LIB is constructed. The experimental results show that the self-discharge effect-2-RC (SDE-2-RC) model can achieve higher accuracy in simulating the working state of the battery, and the peak error of the simulated voltage is only 0.04342V, and the accuracy can reach more than 98.966%. Using LM-MILS and adaptive Kalman filtering algorithm (AEKF) for the state of charge (SOC) estimation, the results show that the algorithm has a fast convergence speed and strong tracking performance. The maximum SOC estimation errors in HPPC, DST, and BBDST three operating conditions are 0.00929, 0.01273, and 0.01002, respectively. The fluctuation range is small, and the maximum estimation error is less than 2%, which verifies that the improved parameter identification algorithm has good performance in improving the SOC estimation accuracy of LIB.

Keywords: Lithium-ion battery; LM-MILS algorithm; SDE-2-RC equivalent model; Online parameter identification

*Corresponding author: Shunli Wang. Tel: +86-15884655563. E-mail address: 497420789@qq.com.

1. Introduction

In the past few decades, due to increasing environmental pollution and increasingly serious energy consumption[1], renewable and clean energy has become the focus of energy research[2]. The development of electric vehicles has become a leading industry in the field of new energy, and electric drive vehicles such as hybrid electric vehicles (HEV), plug-in hybrid electric vehicles (PHEV), and extended-range electric vehicles (E-REV) have emerged[3]. At the same time, the rapid development of electric vehicles has greatly promoted the development of energy storage science and technology and the battery industry[4]. Lithium batteries have attracted extensive attention due to their long cycle life, strong charging capability, wide operating temperature range, and strong endurance[5]. Due to the characteristics of single use and group use of lithium batteries, it has brought new challenges to the safety of power battery management systems (BMS)[6], and it is still a technical bottleneck for the promotion and development of new energy electric vehicles[7-10]. The functional requirements of BMS can be divided into four parts: scientific control strategy, accurate performance management, communication management, and fault diagnosis, and the performance management part involving LIB state estimation is particularly important[11, 12].

At present, LIB equivalent modeling research is a very broad research field, which has spawned a variety of modeling techniques[13], such as electrochemical models, artificial intelligence models, thermodynamic models, and equivalent circuit models (ECM)[14]. Electrochemical models usually involve a large number of equations and characteristic parameters, which are computationally intensive and difficult[15]. The artificial intelligence model needs to invest a lot of cost in software and hardware to meet the needs of timely updating[16, 17], and it is difficult to be widely used in BMS management. The ECM model has been widely used because of its simple structure and reasonable accuracy[18].

In the current field of LIB research, the most commonly used and basic models include the internal resistance model, the Thevenin model, the PNGV model, and the second-order RC model[19, 20]. These basic models can meet some application scenarios that do not require high model parameter accuracy. For example, the internal resistance model circuit is simple and the parameters are easy to determine, but it cannot characterize the dynamic working process of the LIB[21]. The Thevenin model has a clear physical meaning. It uses resistance and capacitance equivalent to the capacitive impedance in the battery. However, the resistance in the model is a fixed value, which has certain drawbacks[22, 23]. The PNGV model adds capacitance to the Thevenin model and considers the effect of current on OCV. The second-order RC model uses two RC loops to represent the electrochemical polarization and concentration polarization effects of the battery during charging and discharging, respectively. Compared with other models, the second-order RC model has higher accuracy and a wider application range[24, 25]. To realize ECM with higher accuracy and richer application scenarios, many researchers have made a lot of efforts.

In order to solve the problems existing in aviation batteries working in a high-complexity environment, Wang et al.[26] proposed a spliced equivalent circuit model (S-ECM) through experimental research on the working characteristics of LIB packs, which realized the special working conditions and accurate mathematical expression of LIB packs. The experimental results show that the parameter identification results of the S-ECM model are in good agreement with the performance of aviation LIB, and the voltage tracking error is less than 2%. Ji et al.[27] presented a variable resistance-capacitor second-order RC equivalent circuit model. To explore the influence of fixed-value resistance and variable

capacitance in ECM, the exponential fitting method and the pulse discharge method were used to identify the model parameters and constructed the second-order equivalent model of variable resistance and capacitance is developed. The results show that the accuracy of the variable RC model they constructed can reach 97.1%, which is 3.3% higher than that of the fixed RC second-order model. Since the heat generated from the circuit during the operation of the LIB will affect the parameters of the battery model, more and more researchers have begun to explore how to effectively solve the impact of the battery thermal effect. To solve such problems, Cai et al.[28] identified the thermal characteristic parameters at different temperatures by measuring the relevant factors such as the surface temperature of the lithium battery and the ambient temperature according to the principle of heat transfer and the calorific value of the battery. Based on the model, an ECM considering the thermal characteristics of the LIB is established. The results show that the estimated temperature of the electrical model and the actual temperature of the battery have good followability, and the maximum relative error is within 5%. In order to break through the limitation of computing power and storage space of traditional battery management, Wang et al.[29] established a digital twin model of LIB based on networked BMS architecture based on cloud collaboration and digital twin technology. The results show that the digital twin model can overcome the shortcomings of traditional battery management systems using fixed parameters through online learning, and achieve accurate management and ideal performance for the full life cycle of LIB. Mevawalla et al.[30] proposed a one-dimensional partial differential model based on physical and chemical diffusion, which can quickly and accurately predict the voltage and temperature according to the operating state of LIB, which is helpful for the precise thermal design and thermal design of LIB management.

In the application process of ECM, high-precision ECM parameters can ensure the fidelity of its model. Many factors affect the accuracy of ECM parameters, such as temperature, state of charge, remaining battery life, etc. How to obtain high-precision, high-real-time degree of ECM parameters has become the focus of researchers. Wei et al.[31] innovatively proposed a degree of freedom (DOF) canceller, and combined it with Frisch format recursion, aiming at the fact that the unexpected perception of noise may affect the identification of ECM parameters in practical applications. Estimate noise statistics and model parameters. The results show that the method can effectively reduce the parameter identification deviation caused by noise, and the anti-interference ability and model accuracy are greatly improved. To balance the accuracy and real-time performance of ECM parameter identification. Wu et al.[32] proposed a self-adjusting multiple forgetting factor recursive least-squares method (AMFFRLS) based on forgetting factor recursive least squares (FFRLS) to update model parameters in real-time. The experimental results show that the AMFFRLS algorithm has smaller errors under different working conditions, and its performance is better than that of the FFRLS algorithm. In order to ensure high modeling accuracy and SOC estimation accuracy, Bian et al.[33] used particle swarm optimization algorithm to optimize the online parameters of ECM parameters and the covariance matrix of extended Kalman filter (EKF) and the simulated voltage error could be limited to -0.03V to 0.03V range. Compared with the ECM offline parameter identification method, the above method has higher real-time performance and lower complexity. However, due to the complexity of the recurrence formula of the degree of freedom canceller in the literature [31], the particle swarm optimization algorithm in the literature [33] has a large amount of calculation and usually requires high hardware support, so it is difficult to apply to the actual BMS parameters. estimate. The maximum and minimum forgetting factors in [32] vary with the battery operating conditions and are not suitable for online parameter identification.

To establish an ECM with higher parameter accuracy, this study focuses on solving the self-

discharge effect of LIB, and innovatively establishes the SDE-2-RC model to characterize the self-discharge process in detail. It is verified by experiments that the SDE-2-RC model can more accurately simulate the LIB working process. To solve the data redundancy phenomenon in the online parameter identification algorithm, an innovative LM-MILS algorithm is proposed, which improves the accuracy of online parameter identification by limiting the data memory length and expanding the innovation vector, and the Hybrid Pulse Power Characterization (HPPC) experiment and the Beijing Bus Dynamic Stress Test (BBDST) experiment are used to verify the accuracy of the improved model[34]. The online SOC estimation based on the LM-MILS and AEKF algorithms provides the experimental basis and theoretical basis for the accurate state estimation and wide application of LIB.

The rest of this research is organized as follows: Section 2 mainly introduces the SDE-2-RC equivalent circuit structure of the LIB and the overall structure of the LM-MILS online parameter identification algorithm. Section 3 mainly includes the parameter identification results of the SDE-2-RC equivalent model and the verification of the identification accuracy. Section 4 verifies the improvement effect of the LM-MILS algorithm on the SOC estimation accuracy under three different working conditions. Finally, a summary is described in Section 5.

2. Theoretical Analysis

2.1 Battery Equivalent Model Establishment

At present, most of the commonly used lithium battery ECMs improve the accuracy of the ECM by solving the thermal effect and noise effect of the LIB, or by increasing the order of the RC network[35, 36]. Most researchers ignore the self-discharge effect of the LIB. In the state of slow discharge, the open-circuit voltage will also change with the resting time. If this slight change is ignored, the parameter accuracy of the ECM will also be affected to a certain extent. After a detailed study of the working characteristics of the LIB, to reduce the influence of the parameter accuracy caused by the change of the open-circuit voltage, the SDE-2-RC model was constructed in this study. The SDE-2-RC model is shown in Fig. 1.

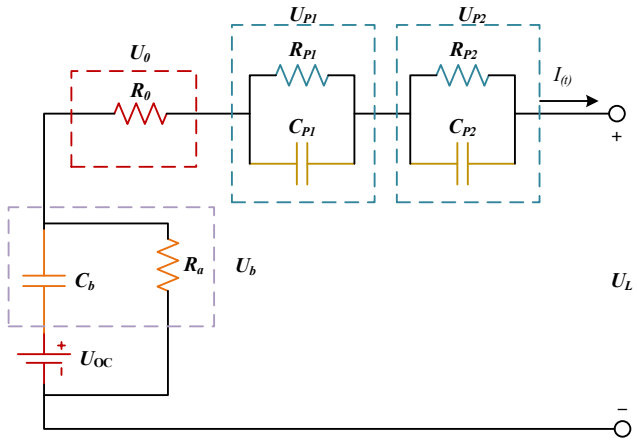

Fig. 1 SDE-2-RC open-circuit model

Based on the 2-RC model, the SDE-2-RC model uses the self-discharge loop composed of C_b and R_a to effectively characterize the self-discharge effect. In Fig. 1, U_L represents the terminal voltage of LIB, $I($ t) is the circuit loop current, the two RC loops composed of R_{P1}, C_{P1}, and R_{P2}, C_{P2} are used to

characterize the electrochemical polarization effect and concentration polarization effect of the battery respectively, R_0 is the ohmic internal resistance. According to Kirchhoff's voltage law, the voltage relationship in the SDE-2-RC circuit is shown in Equation (1).

$$\begin{cases} U_L = U_{oc} - U_b - U_0 - U_{p1} - U_{p2} \\ i_L = C_{p1}\dfrac{dU_{p1}}{dt} + \dfrac{U_{p1}}{R_{p1}} = C_{p2}\dfrac{dU_{p2}}{dt} + \dfrac{U_{p2}}{R_{p2}} \end{cases} \tag{1}$$

Accurate identification of the characteristic parameters in the self-discharge loop is an essential prerequisite for characterizing the self-discharge effect of LIBs. The method of parameter identification will be introduced in the following. When the SOC drops to 0.5, the voltage change curve when the battery is charged and discharged can be drawn, as shown in Fig. 2.

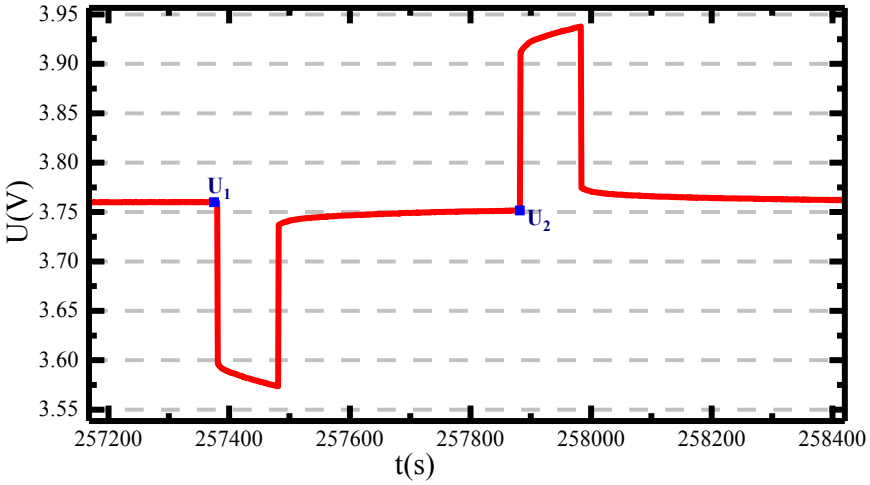

Fig. 2 Charge-discharge cycle at SOC=0.5

In the self-discharge loop of the LIB, C_b can be used to represent the voltage change due to the current accumulation effect. The calculation of C_b is shown in Equation (2), and the calculation method is to obtain the average value of C_b from the data of multiple HPPC charge-discharge cycles. In Equation (2), I is the discharge current, U_1 is the instantaneous voltage of discharge, and U_2 is the instantaneous voltage of charging.

$$U_1 - U_2 = \frac{1}{C_b}\int I dt \tag{2}$$

In order to realize the accurate identification of self-discharge resistance R_a, In a constant temperature experimental box, a fully charged LIB was placed and the load was not connected, and the change in open circuit voltage was continuously recorded every day for 45 days. U_b represents the change of LIB open-circuit voltage, and its calculation formula is shown in Equation (3).

$$U_b = \Delta U_{oc} = U_{oc0}\left(1 - e^{-\frac{t}{R_a C_b}}\right) \tag{3}$$

In Equation (3), U_{oc0} is the open-circuit voltage after the battery is fully charged, t represents the discharge time of the battery in the resting state. After calculating the open-circuit voltage change and the corresponding time, the value of R_a can be calculated by Equation (4).

$$R_a = \frac{-t}{C_b \times \ln\left(1 - \frac{\Delta U_{oc}}{U_{oc0}}\right)} \tag{4}$$

SOC_0 generally, takes 1, which represents the battery SOC when fully charged, combined with Equation **Error! Reference source not found.**, the SOC at the current moment can be calculated.

$$SOC_k = SOC_0 - \frac{\eta \int_0^k i(t)\,dt}{Q_0} \tag{5}$$

In Equation (6), η is the discharge efficiency of the LIB, usually $\eta = 1$ at room temperature. Q_0 represents the rated capacity of the LIB[37]. Through modern control theory, the ECM can be discretized[38], as shown in Equation (6).

$$SOC_k = SOC_0 - \frac{\eta \Delta t}{Q_0} i_k \tag{6}$$

$x_k = [SOC_k, U_{p1,k}, U_{p2,k}, U_b]^T$ is the state space variable, i_k is the input, and $y_k = [U_{L,k}]$ is the output, then the discrete state-space equation of the ECM is shown in Equation (7).

$$\begin{cases} x_{k+1} = \begin{bmatrix} 1 & 0 & 0 & 0 \\ 0 & e^{-\frac{\Delta t}{\tau_1}} & 0 & 0 \\ 0 & 0 & e^{-\frac{\Delta t}{\tau_2}} & 0 \\ 0 & 0 & 0 & 1 \end{bmatrix} x_k + \begin{bmatrix} -\frac{\Delta t}{Q_N} \\ R_{P1}\left(1 - e^{-\frac{\Delta t}{\tau_1}}\right) \\ R_{P2}\left(1 - e^{-\frac{\Delta t}{\tau_2}}\right) \\ \frac{1}{C_b} \end{bmatrix} i_k + w_k \\ y_k = U_{oc,k} - R_0 i_k + \begin{bmatrix} 0 \\ -1 \\ -1 \\ -1 \end{bmatrix} x_k + v_k \end{cases} \tag{7}$$

In Equation (7), Δt is the discrete sampling interval; $\tau_1 = R_{p1}C_{p1}$, $\tau_2 = R_{p2}C_{p2}$; w_k is the noise variable; and v_k is the voltage error of each estimate.

2.2 Limited memory multi-innovation least-squares method

After obtaining the characteristic parameters of the self-discharge circuit, R_a and C_b are used as constants in the subsequent identification, and the remaining parameters in the model can be identified by the online parameter identification method. Compared with the offline identification method, the online parameter identification method has lower operational complexity and higher efficiency[39]. Calculation errors are less prone to occur. The recursive least squares (RLS) method has a fast convergence speed and

is simple and efficient for parameter identification. It has been widely used in the field of parameter identification. Equation (8) is the expression for RLS.

$$y(k)=\varphi(k)\theta^{T}(k-1)+e(k) \tag{8}$$

In Equation (8), $\varphi(k)$ is the data vector, $e(k)$ is the observation noise, and $\theta^{T}(k-1)$ is the estimated value of the parameter vector. Take the objective function $J(\theta)$. The purpose of the least-squares method is to find $\hat{\theta}$. When $\theta=\hat{\theta}$, $J(\theta)$ takes the minimum value. Equation (9) is the calculation formula of the objective function and a parameter estimation value of the RLS system.

$$\begin{cases} J(\hat{\theta})=[y(k)-\varphi(k)\hat{\theta}(k)]^{T}[y(k)-\varphi(k)\hat{\theta}(k)] \\ \hat{\theta}=[\varphi(k)\varphi(k)^{T}]\varphi(k)y(k) \end{cases} \tag{9}$$

To improve the accuracy of parameter identification in the iterative calculation process, it is necessary to update the input and output experimental data in real-time when RLS is used for simulation calculation. To increase the accuracy of data utilization and introduce innovation $v(k)$ to reduce the possibility of large errors, the scalar innovation of the system can be shown in Equation (10).

$$v(k)=y(k)-\varphi(k)\theta(k-1)^{T} \tag{10}$$

The innovation is the difference between the system output observation value at the current moment and the system parameter identification value at the previous moment, and the innovation can correct the parameter identification result at the previous moment in the identification process. However, with the increase in the number of iterations, the RLS algorithm will appear "data saturation", which reduces the information obtained by the algorithm from the new data, results in a gradual weakening of the correction ability, makes the time-varying system unable to track the parameters well, and eventually, the error of parameter identification is getting bigger and bigger. To solve the above problems, this research adopts the LM-MILS algorithm to identify the parameters of the improved model. The LM-MILS algorithm is based on the RLS identification algorithm and estimates the output at time k according to the $N+1$ groups of data from time $k-N$ by time k and the input data at time $k-1$. The calculation formula is as Equation (11).

$$\begin{cases} K_{k-N,k}=\dfrac{P_{k-N,k-1}\varphi_{k-N}(p,k)}{1+\varphi_{k-N}{}^{T}(p,k)P_{k-N,k-1}\varphi_{k-N}(p,k)} \\ P_{k-N,k}=P_{k-N,k-1}\left[1-K_{k-N,k}\varphi_{k-N}{}^{T}(p,k)P_{k-N,k-1}\right] \\ \theta_{k-N,k}=\theta_{k-N,k-1}+K_{k-N,k-1}V(p,k) \end{cases} \tag{11}$$

In each iteration, the nearest $N+1$ groups of data are selected, and the data before $N+1$ are discarded. The scalar innovation is extended to vector innovation, the data vector is extended to the information matrix, and the expression formula of vector innovation is as follows:

$$V(p,k)=\begin{bmatrix} y(k)-\varphi(k)\theta^{T}(k-1) \\ y(k-1)-\varphi(k-1)\theta^{T}(k-1) \\ \\ y(k-p+1)-\varphi(k-p+1)\theta^{T}(k-p+1) \end{bmatrix} \tag{12}$$

In Equation (12), p is the innovation length. When p is equal to 1, the MILS algorithm is reduced to the RLS algorithm. Generally speaking, it is reasonable to assume that $\theta^{T}(k-1)$ is updated at time $k-1$ close to θ. The LM-MILS algorithm solution formula can be obtained after deduction:

$$\begin{cases} K_{k-N+1,k+1} = \dfrac{P_{k-N,k}\varphi_{k-N}(p,k+1)}{1+\varphi_{k-N}{}^{T}(p,k+1)P_{k-N,k}\varphi_{k-N}(p,k+1)} \\ P_{k-N+1,k+1} = P_{k-N,k}\left[1-K_{k-N+1,k+1}\varphi_{k-N}{}^{T}(p,k+1)P_{k-N,k}\right] \\ \theta_{k-N+1,k+1} = \theta_{k-N,k} + K_{k-N,k}V(p,k) \end{cases} \tag{13}$$

In Equation (13), $\varphi_{(k-N)}(p,k+1)$ represents the expansion of the observation data vector into the observation data matrix of $N+1$ moments. $K_{k-N+1,k+1}$ represents the gain matrix calculated from the data from time $k-N+1$ to time $k+1$.

Forgetting factor recursive least squares (FFRLS) uses the forgetting factor λ to give a larger weight to the data with a longer running time and a smaller weight to the data of the latest time[7-9], to improve the phenomenon of "data saturation" and rationally allocate and utilize data information. It is similar to the FFRLS algorithm, the LM-MILS algorithm limits the output of the data, discards the data with a longer running time, saves the data at the latest time, and estimates the output at the current time through a limited set of data, to ensure the accuracy of obtaining information from the data. Availability and real-time. From the perspective of innovation correction, the LM-MILS algorithm uses a lot of innovation in each recursive calculation. Compared with the RLS and FFRLS algorithms that only use the data contained in one innovation point, the accuracy of parameter estimation can be significantly improved, and the LM-MILS flowchart is shown in Fig. 3.

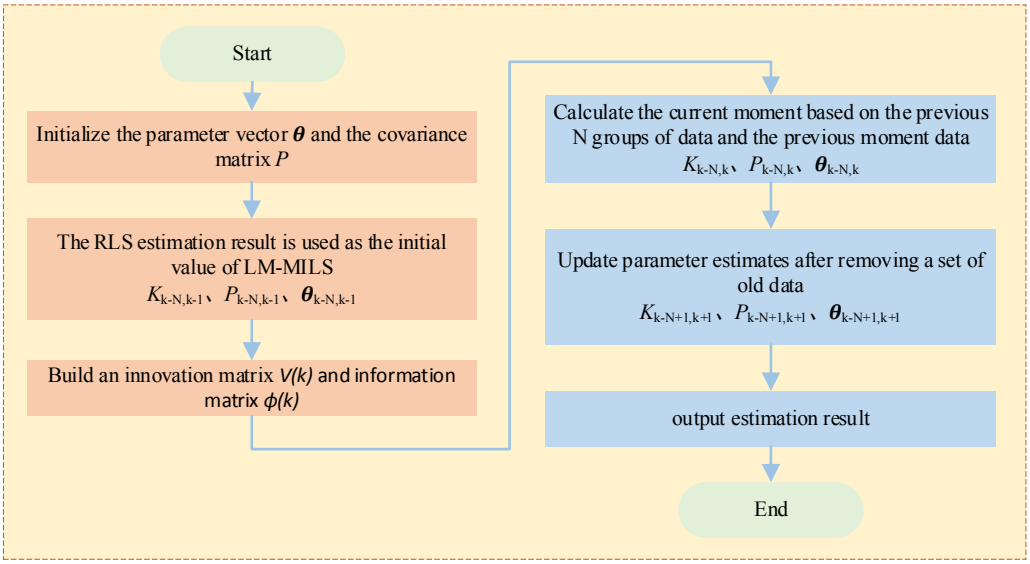

Fig. 3 The flow chart of the LM-MILS

The process of the LM-MILS algorithm is mainly divided into four steps: first, the initialization of the parameters and the estimated values obtained by the RLS algorithm are used to calculate the parameters of the previous moment. Innovation vectors and information matrices and store $N+1$ sets of data are created. The parameter value at the current moment according to the previous $N+1$ groups and the data are estimated at the previous moment. Finally, the parameters for the next moment are calculated according to the current estimated value.

2.3 SOC estimation algorithm

Accurate SOC estimation of LIB is one of the important prerequisites for the safe operation of BMS, and accurate SOC estimation can provide a more scientific battery usage strategy. In the process of SOC

estimation, it is often affected by external factors such as noise and equipment operating conditions, resulting in a decrease in the accuracy of SOC estimation. The traditional extended Kalman filter algorithm is easily affected by the noise covariance of the state equation and the observation equation, and the noise covariance is often set manually, so the adaptive extended Kalman filter algorithm can effectively solve the problem of noise for SOC estimation. influences. Combining the LM-MILS parameter identification algorithm proposed above with the AEKF algorithm can achieve a more accurate SOC estimation.

Compared with EKF, the advantage of AEKF is that it can update the noise matrix q_{k+1}、Q_{k+1}、r_{k+1}、R_{k+1} in real-time to achieve the purpose of continuously correcting the SOC. The updated equations for noise are shown in Equations (14) to (17).

$$q_{k+1} = (1-d_k)q_k + d_k G(\hat{x}_{k+1} - A\hat{x}_{k+1} - Bu_k) \tag{14}$$

$$Q_{k+1} = (1-d_{1-k})Q_k + d_k G(L_{k+1}\varepsilon_{k+1}\varepsilon_{k+1}^T L_{k+1}^T + P_k - AP_{k+1|k}A^T)G^T \tag{15}$$

$$r_{k+1} = (1-d_{1-k})r_k + d_k(y_{+1} - C\hat{x}_{k+1|k} - Du_k - d) \tag{16}$$

$$R_{k+1} = (1-d_{1-k})R_k + d_k(\varepsilon_{k+1}\varepsilon_{k+1} - CP_{k+1|k}C^T) \tag{17}$$

In Equations (14) to (17), $G = (\Gamma^T\Gamma)^T$, Γ is the noise driving matrix, $d_k = \frac{1-b}{1-b^{k+1}}$; b is the forgetting coefficient, $0 < b < 1$. Fig. 4 is a flowchart of SOC estimation using the LM-MILS algorithm and the AEKF algorithm.

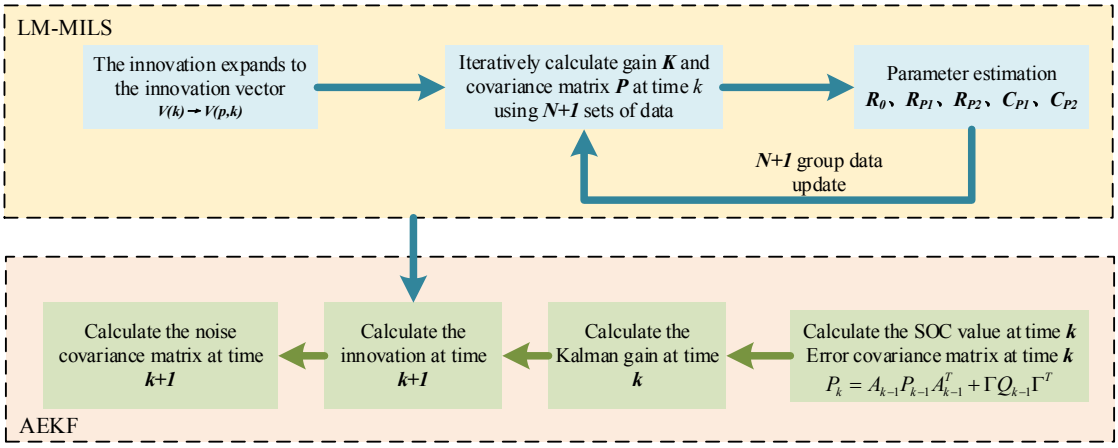

Fig. 4 SOC estimation method based on LM-MILS-AEKF

After the ECM parameter identification is completed using the LM-MILS algorithm, the real-time parameters are input into the AEKF for iterative calculation of the SOC. The SOC estimation at each moment is the parameter estimation value used at the current moment, which ensures the real-time performance of the SOC estimation.

3. Equivalent circuit model validity verification

The ternary LIB is taken as the research object, its rated capacity is 40Ah, and the actual capacity is 39.94Ah measured by the capacity calibration experiment. The experimental platform was built through the BTS200-100-104 battery testing equipment and temperature control box provided by Shenzhen Yakeyuan Technology Co., Ltd. to obtain relevant experimental data. The LIB experimental instrument is shown in Fig. 5.

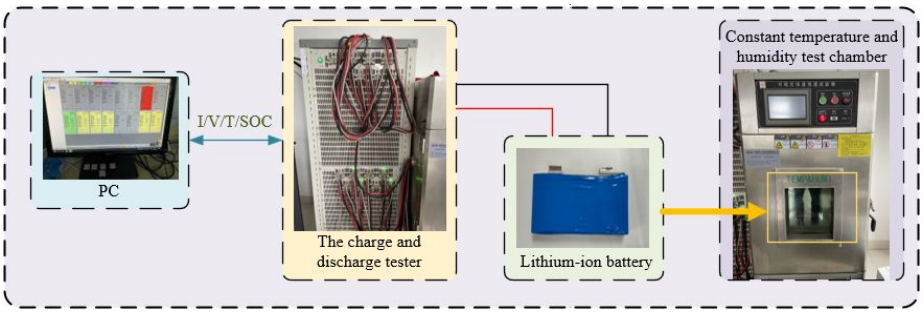

Fig. 5 Experimental lithium-ion battery test platform

3.1 Characteristic parameter identification of self-discharge circuit

The battery was placed in an incubator, and the change in open circuit voltage was measured daily for 45 days. The change in open circuit voltage is shown in Tab. 1. After 45 days of recording, the initial open-circuit voltage U_{oc0} of the LIB is 4.1871V, and the open-circuit voltage U_{oc} drops to 4.1527V. Take $t = 3888000s$. According to Equation (2) to Equation (4), the value of C_b can be calculated, and the average value of C_b is $20118.18394kF$, and $R_a = 35.6596\Omega$ is calculated on this basis.

Tab. 1 Open circuit voltage change within 45 days

U/V									
June.8	4.1871	June.17	4.1739	June.26	4.1662	July.5	4.1601	July.14	4.1561
June.9	4.1866	June.18	4.1731	June.27	4.1656	July.6	4.1594	July.15	4.1557
June.10	4.1860	June.19	4.1724	June.28	4.1650	July.7	4.1591	July.16	4.1552
June.11	4.1832	June.20	4.1720	June.29	4.1644	July.8	4.1588	July.17	4.1550
June.12	4.1821	June.21	4.1711	June.30	4.1632	July.9	4.1582	July.18	4.1546
June.13	4.1802	June.22	4.1702	July.1	4.1627	July.10	4.1579	July.19	4.1541
June.14	4.1791	June.23	4.1689	July.2	4.1621	July.11	4.1577	July.20	4.1533
June.15	4.1777	June.24	4.1683	July.3	4.1615	July.12	4.1573	July.21	4.1531
June.16	4.1756	June.25	4.1674	July.4	4.1609	July.13	4.1566	July.22	4.1527

3.2 Parameter identification verification analysis

OCV refers to estimating the current battery capacity of a battery by measuring the interruption voltage of the battery in the open-circuit state. Since the battery is in a static state for a long time, its port voltage and SOC have a relatively stable functional relationship, so a relatively real SOC estimation value can be obtained through OCV.

The experimental process is: fully charge the battery, then discharge it to a specific SOC value with constant current, and wait for the battery to reach a stable state after standing for a certain time. The battery is discharged in turn at 10% of the rated capacity each time, and the OCV value corresponding to the SOC value is measured after stabilization. Until the SOC is 0, the complete discharge OCV-SOC curve is obtained.

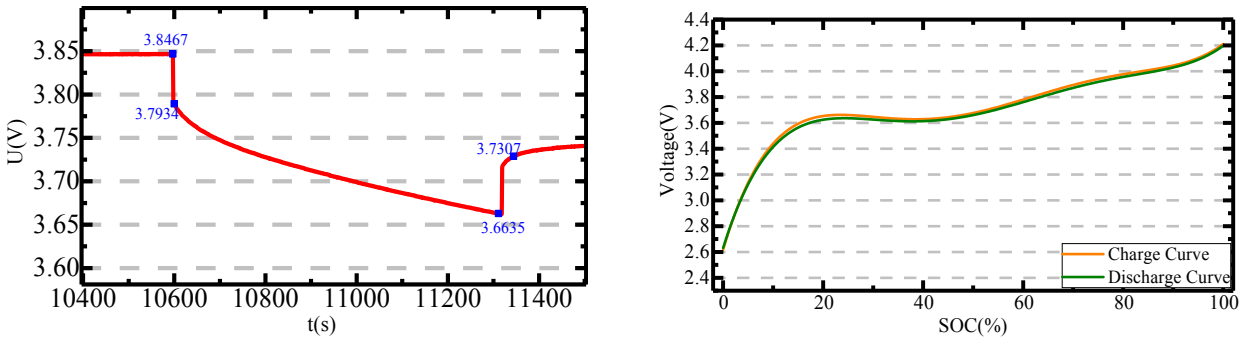

(a)OCV at SOC=0.6 (b)OCV-SOC curve

Fig. 6 Hysteresis characteristic curve of battery OCV

It can be seen from Fig. 6(a) that when the SOC is 0.6, the OCV is 3.7307V. Even if the battery is charged and discharged in the same way, due to the hysteresis effect of the battery, the OCV-SOC fitting curves of the charge and discharge are not completely consistent, but a band-like hysteresis structure with gaps at both ends will be formed.

In the actual use of LIB, the batteries are mostly in the intermittent repetitive charging and discharging process. The HPPC experiment includes intermittent charging and discharging, shelving, and other processes. It has strong dynamics and can well simulate the actual working process of LIB.

The HPPC experiment was carried out at room temperature to obtain the experimental data, and the model parameters were identified online. The experimental steps of HPPC are as follows.

(1) The LIB is charged with constant current and constant voltage at a voltage of 4.2V and a current of 1C until fully charged.

(2) Discharge at 1C constant current for 10 seconds, then put the battery on hold for 40 seconds. To restore the battery to its pre-discharge level, charge it with a constant current of 1C for 10 seconds, and shelve it for 3 minutes after charging.

(3) Discharge the battery at 1C constant current for 6 minutes to reduce the charge by 10%. Repeat steps (2) and (3) 10 times until the battery level reaches 0.

Based on the experimental data obtained under the HPPC condition at room temperature, the LM-MILS algorithm is used to verify the accuracy difference between the SDE-2-RC model and the 2-RC model. Then, based on the SDE-2-RC model, the online parameter identification is carried out through the LM-MILS algorithm, the RLS algorithm, and the FFRLS algorithm, and the simulated voltage is compared with the experimental voltage to verify the accuracy of parameter estimation and the validity of the algorithm. The initial value of online parameter identification will affect the identification accuracy at the initial moment. Even if the initial value of the parameter has a large error, it can be quickly converged in subsequent iterations.

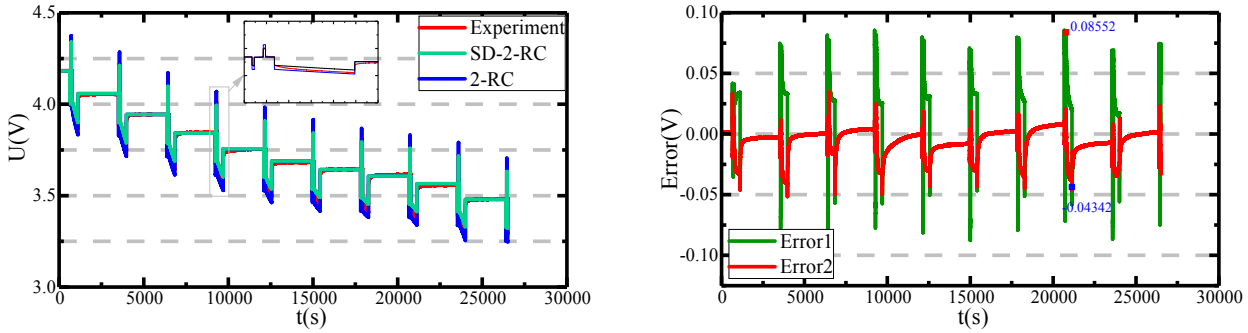

(a) Model comparison under HPPC condition

(b) Model error under HPPC condition

Fig. 7 Model output voltage curve under HPPC condition

Fig. 7 shows the simulated voltage curves of the 2-RC equivalent model and the SDE-2-RC equivalent model after online parameter identification based on the LM-MILS algorithm. In Fig. 7 (a), the 2-RC model has a large fluctuation error during charging and discharging. In contrast, the analog voltage of the SDE-2-RC model has higher accuracy, and the tracking effect is more stable. In Fig. 7 (b), Error1 and Error2 represent the voltage error curves corresponding to the 2-RC model and the SDE-2-RC model, respectively. It can be seen from Fig. 7 (b) that the voltage error is larger each time the cycle starts in the charge and discharge process, this is because the internal chemical reaction of the battery is violent in the initial stage of charge and discharge, and the analog voltage follows the speed slowly. The maximum voltage error of the 2-RC model reaches 0.08522V, and the simulation accuracy is 97.971%. Compared with the 2-RC model, the average voltage error of the SDE-2-RC model is only 0.00758V, and the voltage fluctuation ranges from 0.08552V to -0.08669V is reduced to 0.02097V to -0.04342V, and the simulation accuracy reaches 98.966%, which proves that the SDE-2-RC model can more accurately characterize the complex working characteristics of LIB.

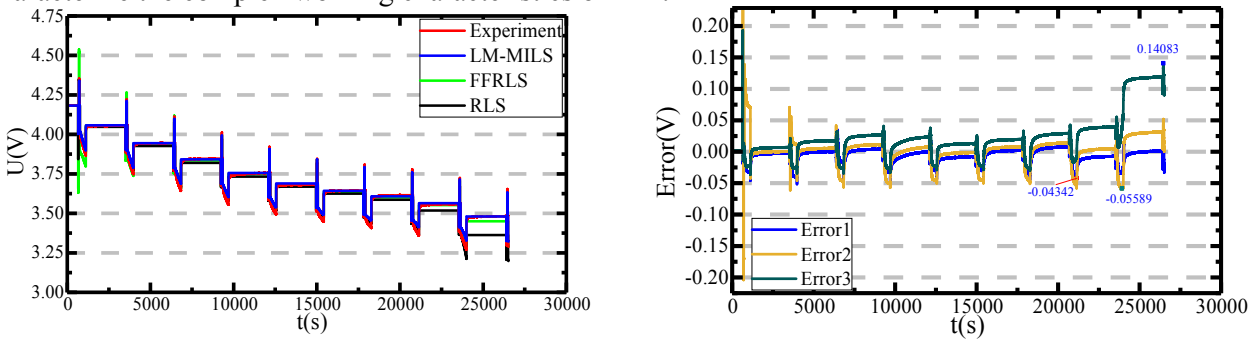

(a) Comparison of parameter identification results under HPPC condition

(b) Parameter identification error under HPPC condition

Fig. 8 Parameter identification results under HPPC working condition

It can be seen from Fig. 8 (a) that in the estimation process, the three algorithms can better track the experimental voltage. However, both the RLS algorithm and the FFRLS algorithm are affected by the phenomenon of "data saturation" to varying degrees. In Fig. 8 (b), Error1 represents the analog voltage error corresponding to the LM-MILS algorithm, Error2 represents the analog voltage error corresponding to the FFRLS algorithm, and Error3 represents the analog voltage error corresponding to the RLS algorithm. It can be seen that the identification error in the initial stage is relatively large. All algorithms can quickly converge to close to the true value, but as the amount of data iteratively increases, the phenomenon of "data saturation" in the RLS algorithm becomes more and more obvious, the estimation error increases with time, and the maximum error reaches 0.14083V. Although the FFRLS algorithm can

better overcome the phenomenon of "data saturation", the estimation error fluctuates greatly at the end of the discharge stage, and the absolute value of the maximum error is 0.05589V. The LM-MILS algorithm can track the measured voltage very well, overcome the phenomenon of "data saturation" to a large extent, and have high estimation accuracy. After the estimation becomes stable, the absolute value of the maximum error is reduced to 0.04342V, accounting for the nominal 1.004% of the voltage, which proves that the LM-MILS algorithm has high accuracy.

4. Analysis of results

4.1 Experimental analysis of HPPC working conditions

The experimental data under HPPC conditions are used to verify the SOC estimation of different algorithms. The comparison is shown in Fig. 9 (a) and Fig. 9 (b).

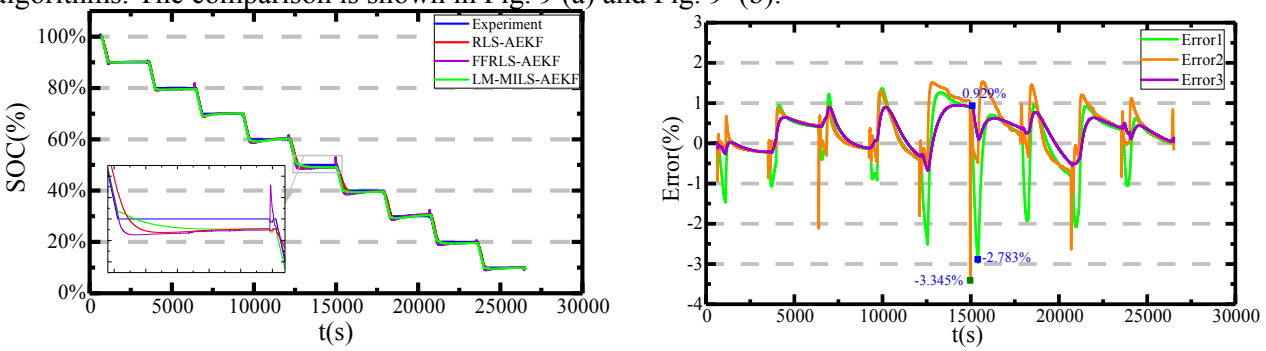

(a) SOC estimation results under HPPC condition (b) SOC estimation error under HPPC condition

Fig. 9 SOC estimation results and errors of HPPC condition

From the enlarged view in Fig. 9 (a), it can be seen that the LM-MILS-AEKF algorithm has the fastest convergence speed and can maintain good stability when starting to discharge. In Fig. 9 (b), Error1 to Error3 correspond to RLS-AEKF, FFRLS-AEKF, and LM-MILS-AEKF estimation errors, respectively. It can be seen that although the "data saturation" phenomenon of online parameter identification is unavoidable, the estimation errors of the three estimation methods in the middle and later stages of the experiment are somewhat different. However, the fluctuation range error of Error3 is smaller than that of Error1 and Error2, and the error fluctuation tends to be stable. The maximum error is 0.929%, and the estimation accuracy can reach 99.071%. Under the HPPC condition, through the Root-mean-square Error (RMSE) and Mean Absolute Error (MAE), as shown in Tab. 2, it is proved that the LM-MILS algorithm has higher accuracy and can better suppress the "data saturation" phenomenon.

Tab. 2 Comparison of different algorithms under HPPC conditions

Contrast method	RLS-AEKF	FFRLS-AEKF	LM-MILS-AEKF
MAE	2.10%	1.71%	0.57%
RMSE	2.91%	1.90%	0.98%

4.2 Experimental analysis of DST working conditions

To verify the validity of the LM-MILS algorithm, the experimental data under the custom DST condition is used for verification. The simulation results of SOC estimation using three online identification algorithms combined with the AEKF algorithm are shown in the figure below.

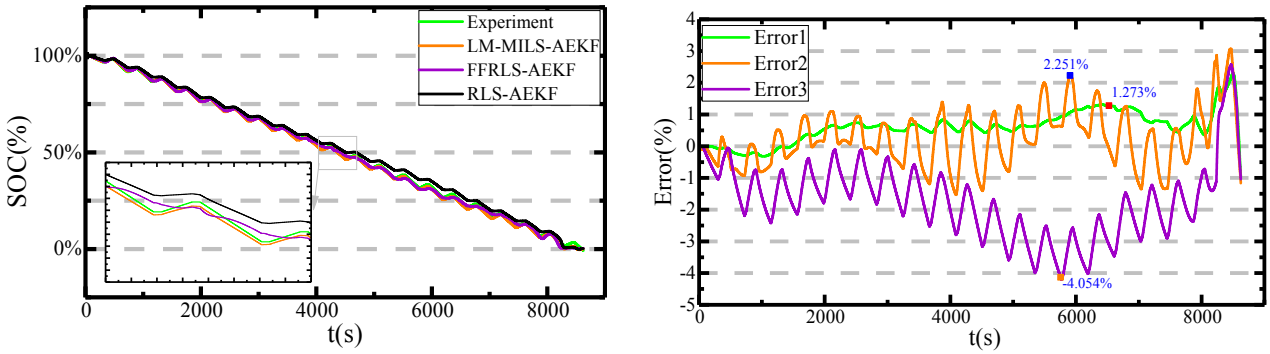

(a) SOC estimation results under DST condition (b) SOC estimation error under DST condition

Fig. 10 SOC estimation results under DST operating condition

In Fig. 10 (a), when changing the working state of the battery, the tracking performance of the LM-MILS-AEKF algorithm is better than that of the RLS-AEKF algorithm and the FFRLS-AEKF algorithm, and the estimated results of the RLS-AEKF algorithm deviate more from the true value in the middle of the experiment. In Fig. 10 (b), Error1 to Error3 correspond to LM-MILS-AEKF, FFRLS-AEKF, and RLS-AEKF estimation errors, respectively. As the battery discharge time goes on, due to the defects of the RLS and FFRLS algorithms themselves, the estimation error gradually increased, and during each charge-discharge state transition, Error2 and Error3 fluctuated violently, while Error1 fluctuated significantly more gently, which could be maintained at in the range of -0.29% to 1.273%, the estimation accuracy is 98.727%, which proves that the LM-MILS-AEKF algorithm has better SOC estimation results. Table 3 shows the comparison of MAE and RMSE of the three algorithms.

Tab. 3 Comparison of different algorithms under DST conditions

Contrast method	RLS-AEKF	FFRLS-AEKF	LM-MILS-AEKF
MAE	1.719%	0.920%	0.616%
RMSE	2.110%	1.621%	1.202%

4.3 Experimental analysis of BBDST working conditions

The BBDST experiment originates from the real data collection of the Beijing bus dynamic test. Through the experimental settings, it can simulate various operating conditions such as bus start, acceleration, and stop. The actual use of LIB is complex and changeable, and it is more convincing to use BBDST experimental data to evaluate the reliability of the algorithm. The simulation results under the BBDST condition are shown in the following figure.

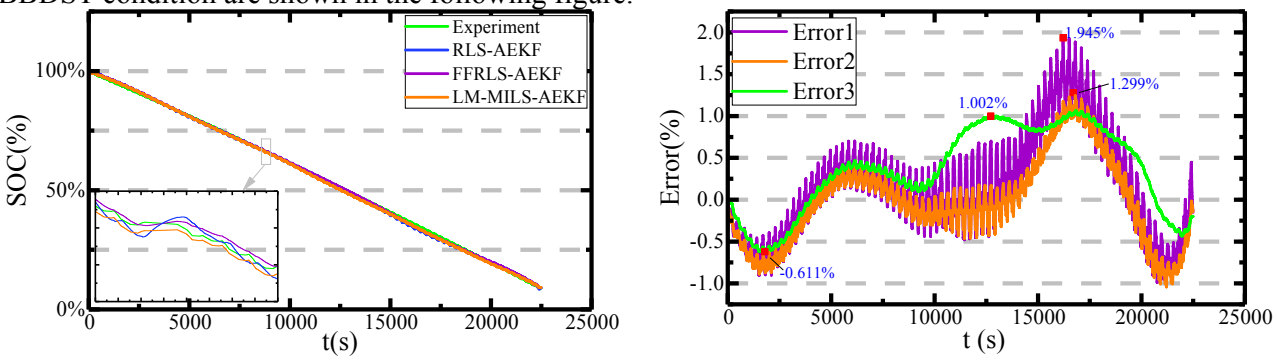

(a) SOC estimation results under BBDST condition (b) SOC estimation error under BBDST condition

Fig. 11 SOC estimation results under BBDST operating condition

Due to the complexity and variability of the working state of the battery under BBDST conditions, it is also difficult to estimate the SOC. It can be seen from the enlarged view of Fig. 11 (a) that the

estimation results of the three algorithms all fluctuate to varying degrees. The fluctuation of RLS-AEKF is the most obvious and the tracking effect is the worst. Error1 to Error3 in Fig. 11 (b) represents estimation errors corresponding to RLS-AEKF, FFRLS-AEKF, and LM-MILS-AEKF. In the initial stage of the experiment, the three error curves have a high degree of coincidence, and the RLS-AEKF estimation error fluctuates greatly. The FFRLS-AEKF error accumulation phenomenon has decreased and the error fluctuation has become smaller, and the maximum error is 1.299%. On the other hand, the LM-MILS-AEKF error has the smallest change, fluctuating in the range of -0.611% to 1.002%, and can also maintain positive tracking when switching between charge and discharge states, with a maximum error of only 1.002%. Under the condition of BBDST, the estimation results of the three algorithms are compared by MAE and RMSE, as shown in Tab.4.

Tab. 4 Comparison of different algorithms under BBDST conditions

Contrast method	RLS-AEKF	FFRLS-AEKF	LM-MILS-AEKF
MAE	1.709%	0.812%	0.357%
RMSE	2.452%	1.800%	1.007%

Through the algorithm verification under the above three complex working conditions, it can be seen that compared with the RLS and FFRLS algorithms, the LM-MILS algorithm can well suppress the phenomenon of "data saturation" and increase the accuracy of online parameter identification to a certain extent. Combining the LM-MILS algorithm with the AEKF algorithm for SOC estimation can greatly improve the SOC estimation accuracy and algorithm stability, and reduce the error fluctuation range.

5. Conclusion

Accurate estimation of the SOC of LIB is the difficulty and focus of the battery management system. Establishing a suitable equivalent model and performing accurate parameter identification can effectively improve the estimation accuracy. To solve the shortcomings of the online parameter identification algorithm and improve the accuracy of model parameter identification. Based on a large number of experiments, this research fully explores the polarization effect and self-discharge effect of LIB, and innovatively establishes the SDE-2-RC equivalent circuit model. When the LIB is not used, the change of the open-circuit voltage is continuously recorded, to complete the identification of the self-discharge characteristic parameters. Then the LM-MILS online parameter identification algorithm is innovatively proposed, by limiting the memory and expanding the innovation matrix to suppress the "data redundancy" phenomenon in the online parameter identification algorithm, so as to achieve the purpose of improving the accuracy of parameter identification.

To verify the validity of the model and algorithm, the verification analysis is carried out in HPPC, DST, and BBDST conditions. The verification results manifest that, based on the same parameter identification algorithm, the SDE-2-RC model can achieve 98.966% simulation voltage accuracy under HPPC conditions, which is 0.995% higher than the traditional second-order RC model; The SOC estimation accuracy of the LM-MILS-AEKF algorithm under the three operating conditions is 99.071%, 98.727%, and 98.998%, respectively. Compared with the traditional algorithm, the estimation performance is superior, the error fluctuation range is significantly reduced, and the estimation accuracy and stability are had improved significantly. The content of this research has positive significance for the accurate parameter identification of the equivalent model and the state detection of LIB, but the accuracy of the SDE-2-RC model and the LM-MILS algorithm is not verified under the condition of considering the temperature change. Due to the increase in the number of charges and discharges, the remaining service life of LIB is reduced, and the parameters of the LIB may change further, which needs to be

further studied in practical applications.

Acknowledgments

The work was supported by the National Natural Science Foundation of China (No. 61801407).

Data Availability Statement

The data that support the findings of this study are available from the corresponding author upon reasonable request.

References

[1] YANG Y, OKONKWO E G, HUANG G, et al. On the sustainability of lithium ion battery industry – A review and perspective [J]. Energy Storage Materials, 2020, 36.

[2] ZHANG H, LIU X, LI H, et al. Challenges and Strategies for High ⊥ nergy Aqueous Electrolyte Rechargeable Batteries [J]. Angewandte Chemie, 2020, 133(2).

[3] CONG L, LIU W, KONG S, et al. A review on end-of-use management of spent lithium-ion batteries from sustainability perspective [J]. 2021, 143(10) : 1-35.

[4] FANG R, CHEN K, YIN L, et al. The Regulating Role of Carbon Nanotubes and Graphene in Lithium-Ion and Lithium-Sulfur Batteries [J]. Advanced Materials, 2019, 31(9).

[5] LIU Z, CHEN S H, WU H F, et al. A Combined State of Charge Estimation Method for Lithium-Ion Batteries Using Cubature Kalman Filter and Least Square with Gradient Correction [J]. Advanced Theory and Simulations, 2022, 5(3).

[6] ZUO H Y, ZHANG B, HUANG Z H, et al. Effect analysis on SOC values of the power lithium manganate battery during discharging process and its intelligent estimation [J]. Energy, 2022, 238.

[7] QIN S, QIN D C, WU H X, et al. State of Charge estimation of lithium-ion power battery based on online parameter identification method and BP neural network [J]. International Journal of Electrochemical Science, 2022, 17(1).

[8] FENG J, WU L, HUANG K, et al. Online SOC estimation of a lithium-ion battery based on FFRLS and AEKF [J]. Energy Storage Science and Technology, 2021, 10(1) : 242-9.

[9] XU Y D, HU M H, FU C Y, et al. State of Charge Estimation for Lithium-Ion Batteries Based on Temperature-Dependent Second-Order RC Model [J]. Electronics, 2019, 8(9).

[10] WEI Z, ZHAO D, HE H, et al. A noise-tolerant model parameterization method for lithium-ion battery management system [J]. Applied Energy, 2020, 268.

[11] WANG Q, WANG Z, ZHANG L, et al. A Novel Consistency Evaluation Method for Series-Connected Battery Systems Based on Real-World Operation Data [J]. Ieee Transactions on Transportation Electrification, 2021, 7(2) : 437-51.

[12] POMERANTSEVA E, BONACCORSO F, FENG X, et al. Energy storage: The future enabled by nanomaterials [J]. Science, 2019, 366(6468).

[13] ZHAO S, GUO Z, YAN K, et al. Towards High-energy-density Lithium-ion Batteries: Strategies for Developing High-capacity Lithium-rich Cathode Materials [J]. Energy Storage Materials, 2020.

[14] JIANG C, WANG S, WU B, et al. A state-of-charge estimation method of the power lithium-ion battery in complex conditions based on adaptive square root extended Kalman filter [J]. Energy, 2021, 219.

[15] BI, YALAN. Online State and Parameter Estimation for Lithium-ion Batteries Based on a Reduced-order Electrochemical Life Model [J]. 2020.

[16] ZHANG L, PENG H, NING Z, et al. Comparative Research on RC Equivalent Circuit Models for Lithium-Ion Batteries of Electric Vehicles [J]. Applied Sciences-Basel, 2017, 7(10).

[17] HAN K, WANG T, ZHANG N, et al. A film coating assembled by tubular nitrogen-doped carbon fibers as an

efficient membrane spacer to suppress the shuttle effect for long-life lithium–sulfur batteries [J]. Electrochimica Acta, 2021, 365(15) : 137232.

[18] XIAO J, LI Q, BI Y, et al. Understanding and applying coulombic efficiency in lithium metal batteries [J]. Nature Energy, 2020, 5(8) : 561-8.

[19] WANG Y J, TIAN J Q, SUN Z D, et al. A comprehensive review of battery modeling and state estimation approaches for advanced battery management systems [J]. Renewable & Sustainable Energy Reviews, 2020, 131.

[20] SHAO L, JIN S. Resilience assessment of the lithium supply chain in China under impact of new energy vehicles and supply interruption [J]. Journal of Cleaner Production, 2020, 252.

[21] WANG Y J, CHEN Z H. A framework for state-of-charge and remaining discharge time prediction using unscented particle filter [J]. Applied Energy, 2020, 260.

[22] CHEN Y, DOU A, ZHANG Y J F I M. A Review of Recycling Status of Decommissioned Lithium Batteries [J]. Frontiers in Materials, 2021, 8: 634667.

[23] DUFFNER F, KRONEMEYER N, TüBKE J, et al. Post-lithium-ion battery cell production and its compatibility with lithium-ion cell production infrastructure [J]. Nature Energy, 2021, 381

[24] TIAN M, AN Z, CHEN X, et al. SOC estimation of lithium battery based online parameter identification and AEKF [J]. Energy Storage Science and Technology, 2019, 8(4) : 745-50.

[25] HE L, HU M K, WEI Y J, et al. State of charge estimation by finite difference extended Kalman filter with HPPC parameters identification [J]. Science China-Technological Sciences, 2020, 63(3) : 410-21.

[26] WANG S, FERNANDEZ C, LIU X, et al. The parameter identification method study of the splice equivalent circuit model for the aerial lithium-ion battery pack [J]. Measurement & Control, 2018, 51(5-6) : 125-37.

[27] JI Y-J, QIU S-L, LI G. Simulation of second-order RC equivalent circuit model of lithium battery based on variable resistance and capacitance [J]. Journal of Central South University, 2020, 27(9) : 2606-13.

[28] CAI Y, CHE Y, LI H, et al. Electro-thermal model for lithium-ion battery simulations [J]. Journal of Power Electronics, 2021, 21(10) : 1530-41.

[29] WANG Y J, XU R L, ZHOU C J, et al. Digital twin and cloud-side-end collaboration for intelligent battery management system [J]. Journal of Manufacturing Systems, 2022, 62: 124-34.

[30] MEVAWALLA A, PANCHAL S, TRAN M K, et al. One dimensional fast computational partial differential model for heat transfer in lithium-ion batteries [J]. Journal of Energy Storage, 2021, 37.

[31] WEI Z B, HE H W, POU J, et al. Signal-Disturbance Interfacing Elimination for Unbiased Model Parameter Identification of Lithium-Ion Battery [J]. Ieee Transactions on Industrial Informatics, 2021, 17(9) : 5887-97.

[32] WU M Y, QIN L L, WU G. State of charge estimation of power lithium-ion battery based on an adaptive time scale dual extend Kalman filtering [J]. Journal of Energy Storage, 2021, 39.

[33] BIAN X L, WEI Z B, HE J T, et al. A Two-Step Parameter Optimization Method for Low-Order Model-Based State-of-Charge Estimation [J]. Ieee Transactions on Transportation Electrification, 2021, 7(2) : 399-409.

[34] STEWART S G, SRINIVASAN V, NEWMAN J. Modeling the performance of lithium-ion batteries and capacitors during hybrid-electric-vehicle operation [J]. Journal of the Electrochemical Society, 2008, 155(9) : A664-A71.

[35] OHZUKU T, BRODD R J. An overview of positive-electrode materials for advanced lithium-ion batteries [J]. Journal of Power Sources, 2007, 174(2) : 449-56.

[36] YE P F, HAN X S, YANG M, et al. A Novel Thevenin Equivalent Model Considering the Correlation of Source-Grid-Load in Power Systems [J]. Ieee Access, 2021, 9: 31276-86.

[37] DING Z, DENG T, LI Z, et al. SOC Estimation of Lithium-ion Battery Based on Ampere Hour Integral and Unscented Kalman Filter [J]. China Mechanical Engineering, 2020, 31(15) : 1823-30.

[38] WANG K, LIU C L, SUN J R, et al. State of Charge Estimation of Composite Energy Storage Systems with Supercapacitors and Lithium Batteries [J]. Complexity, 2021, 2021.

[39] LAI X, GAO W K, ZHENG Y J, et al. A comparative study of global optimization methods for parameter identification of different equivalent circuit models for Li-ion batteries [J]. Electrochimica Acta, 2019, 295: 1057-66.